Computational Modeling of an MRI Guided Drug Delivery System Based on Magnetic Nanoparticle Aggregations for the Navigation of Paramagnetic Nanocapsules

N.K. Lampropoulos · E.G. Karvelas · I.E. Sarris

Abstract A computational method for magnetically guided drug delivery is presented and the results are compared for the aggregation process of magnetic particles within a fluid environment. The model is developed for the simulation of the aggregation patterns of magnetic nanoparticles under the influence of MRI magnetic coils. A novel approach for the calculation of the drag coefficient of aggregates is presented. The comparison against experimental and numerical results from the literature is showed that the proposed method predicts well the aggregations in respect to their size and pattern dependance, on the concentration and the strength of the magnetic field, as well as their velocity when particles are driven through the fluid by magnetic gradients.

Keywords MRI guided drug delivery, Aggregations, Magnetic nanocapsules

1 INTRODUCTION

From the beginnings of 1970s researchers were studying the concept of magnetic guided drug delivery method [1, 2]. The concept of this method is to attach the drug to the micro- or nanoparticles and then to inject them to the bloodstream. For the guidance to the targeted area, a Magnetic Resonance Imaging (MRI) device is needed. By making use of the magnetic guided drug delivery method, the quantity of the drug required to reach therapeutic levels is being reduced. Also, the drug concentration at targeted sites is increased.

The efficiency of this concept depends on the materials of the particles (cobalt and manganese ferrites, encapsulated or coated [3]), the blood flow rate and the intensity of the magnetic field [4]. It is found that, this method is more efficient in small blood vessels with low blood flow rates than large blood vessels, where the flow rate is higher. A small size of particles implies a magnetic response of

Corresponding author: N.K. Lampropoulos, Email : nikolaoslampropoulos@hotmail.com, tel : +30 697 93 86 453, fax : +30 210 53 85 306

Department of Energy Technology, Technological & Educational Institute of Athens, Agiou Spiridonos 17, 12210 Athens

reduced strength and as a result, it is difficult to drive particles and keep them in the targeted region [5]. In order to overcome this difficulty the use of magnetic particles to create aggregations is proposed in order to increase the magnetic response [6]. The total magnetic moment of clusters is higher than that of isolated particles, and therefore, cluster are more magnetically responsive [7]. The ratio of the velocity of the aggregates to the velocity of an individual particle was found to reach a constant value independent of the aspect ratio value [8]. The magnetization of nanospheres increases as a result of the increase in the concentration of matter along the direction of the field. This increase leads to the observed change in velocity [9]. When the aggregations reach the targeted region, they break up into single particles. This break up can be achieved by using superparamagnetic particles that lose the magnetization after moving out from the magnetic field [6]. The size of aggregates is a very important parameter, since large aggregations could form clots in small arteries. On the other hand, a small aggregation would be dragged away from the cardiovascular system circulation. Therefore, the size of aggregation has an important role in the effort to create an efficient propulsion through the blood vessels. Magnetic drug targeting is possible in treating superficially located diseases, such as tumors and vascular diseases. The treatment of tissues located away from the body surface is not possible because the magnetic force decrease with the increasing distance from the electromagnetic coil [10]. In order to overcome this difficulty magnets are implemented near the targeted sites [11, 12].

Since an analytical study of aggregation process is impossible to be developed, a numerical model for magnetically guided drug delivery is attended. The method that is proposed here simulates the movement of aggregated magnetic particles in a fluid environment. The numerical model can simulate the number of resulting aggregations whose size and pattern depend on the concentration and the strength of the magnetic field. The forces acting on a particle are described in detail in Section 2. The model is validated through a comparison with two benchmark test cases of Ref. [6] and Ref. [13] and the results are discussed in Section 3. Finally, discussion and conclusions are presented in Sections 4 and 5, respectively.

2 METHODS

For the propulsion model of the particles, six major forces are considered, i.e. the magnetic force from MRIs Main Magnet static field as well as the Magnetic field gradient force from the special Propulsion Gradient Coils. The static field caters for the aggregation of nanoparticles while the magnetic gradient navigates the agglomerations. Moreover, the contact forces among the aggregated nanoparticles and the wall, and the Stokes drag force for each particle are considered, while only spherical particles are used here. Finally, gravitational forces due to gravity and the force due to buoyancy are added.

The motion of particles are given by the Newton equations:

$$m_i \frac{\partial \boldsymbol{u}_i}{\partial t} = \boldsymbol{F}_{mag\_i} + \boldsymbol{F}_{nc\_i} + \boldsymbol{F}_{tc\_i} + \boldsymbol{F}_{drag\_i} + \boldsymbol{F}_{boy\_i} + \boldsymbol{W}_i \qquad (1)$$

$$\boldsymbol{I}_i \frac{\partial \omega_i}{\partial t} = \boldsymbol{M}_{drag\_i} + \boldsymbol{M}_{con\_i} + \boldsymbol{T}_{mag\_i} \qquad (2)$$

where, the index i stands for the particle i. The bold variables are vectors. The velocity is $\boldsymbol{u}_i$ and the rotational velocity is $\boldsymbol{\omega}_i$. The mass of particle i is m_i, t stands for the time and the mass moment of inertia matrix is $\boldsymbol{I}_i$. The linear and angular acceleration are $\frac{\partial \boldsymbol{u}_i}{\partial t}$ and $\frac{\partial \omega_i}{\partial t}$, respectively. The total magnetic force is $\boldsymbol{F}_{mag\_i}$. $\boldsymbol{F}_{nc\_i}$ and $\boldsymbol{F}_{tc\_i}$ are the normal and tangential contact forces, respectively. $\boldsymbol{F}_{drag\_i}$ stands for the hydrodynamic drag force. $\boldsymbol{F}_{boy\_i}$ and $\boldsymbol{W}_i$ are the buoyancy and the weight forces. $\boldsymbol{M}_{drag\_i}$ and $\boldsymbol{M}_{con\_i}$ stand for the drag and the contact moments, respectively. $\boldsymbol{T}_{mag\_i}$ is the torque due to the magnetic field at the position of particle i.

In the following section, the major forces that are taking into account during the simulation are described in detail.

2.1 Forces acting on particles

1. *Magnetic Forces:* Magnetic forces, $\boldsymbol{F}_{mag\_i}$, exerted on the i particle are given by [14–16] :

$$\boldsymbol{F}_{mag\_i} = \boldsymbol{F}_{intmag\_i} + \boldsymbol{F}_{ismag\_i} \tag{3}$$

where, $\boldsymbol{F}_{intmag\_i}$ is the magnetic force due to the interaction of the ith particle with the magnetic field, and $\boldsymbol{F}_{ismag\_i}$ is the magnetic force acting on the ith particle due to its interaction with the surrounding magnetic particles.
The force $\boldsymbol{F}_{intmag\_i}$ in the volume of the ferromagnetic body, V, is given by:

$$\boldsymbol{F}_{intmag\_i} = V(\boldsymbol{m}_i \cdot \nabla)\boldsymbol{B}_{ext\_i} \tag{4}$$

The force $\boldsymbol{F}_{ismag\_i}$ is given by:

$$\boldsymbol{F}_{ismag\_i} = \sum_{j}^{N} \boldsymbol{F}_{ismag\_ji} \tag{5}$$

The numerical model for the magnetic forces is given in [13].

2. *Fluid Forces:* Each particle is subjected to the drag force that reads as:

$$\boldsymbol{F}_{drag\_i} = \frac{1}{2}\rho u^2 C_d A \tag{6}$$

where, ρ is the density of the fluid, u is the speed of the particle i relative to the fluid and A is the reference area which equals to πr^2, where r stands for the radius of spherical particle. C_d is the drag coefficient given by:

$$\boldsymbol{C}_d = \frac{24\left[1 + 0.15Re^{0.687}\right]}{Re} \tag{7}$$

where, Re is the Reynolds number based on the particle diameter [17].
In the present work, a new model is developed for the substitution of the reference area A, in Eq. (6), with the effective area A_{eff}. This substitution takes into account the fact that the downstream spheres of the chain lie partially in the wake of the upstream one, therefore the reference area A in Eq. (6) of each sphere must be reduced to each real area that is exposed to the flow. On this basis the area A_{eff} can be calculated as follows :
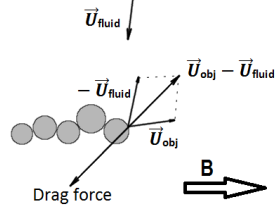
Fig. 1: Relevant velocity and drag force of a particle.

(a) Sweep all spheres.

(b) Find the tangent sphere to the current one.

(c) A straight chain assumption considered where the sphere (1) is tangent only to two spheres namely the upwind and downwind. Sphere (2) which lies upstream to sphere (1) is found out by checking the inner product $\overline{32} * (\mathbf{U}_{obj} - \mathbf{U}_{fluid})$ to be positive, see Figs. 1 and 2a. Where, $\mathbf{U}_{obj}$ stands for the velocity of the sphere and $\mathbf{U}_{fluid}$ stands for the velocity of the fluid

(d) Project the area of spheres (2 and 1) on the plane $\mathbf{U}_{obj} - \mathbf{U}_{fluid}$ that is cross sphere (2) at each center, see Fig. 2b. This yields into two intersected circles, as shown in Fig. 3.

(e) Change to plane coordinate system ($2D$).

(f) Calculate the overlapping area (white domain in Fig. 3). The mathematical formula reads as:

$$E_{overlapping} = domain(234) + domain(134) - E(1234) \tag{8}$$

(g) Substitute Eq. (6) with the equation:

$$\boldsymbol{F}_{drag\_i} = \frac{1}{2}\rho u^2 C_d A_{eff} \tag{9}$$

In this way, the real reference area A_{eff} of sphere exposed to the flow, i.e.:

$$A_{eff} = \pi r_i{}^2 - E_{overlapping} \tag{10}$$

is taken into account.

3. *Collision Forces:* Each particle interacts with other particles through contact. In our model we use the Discrete Element Method (DEM) to calculate the motion of particles [18]. DEM is a numerical model capable of describing the mechanical behaviour of assemblies of spheres and computing the motion and shear effect of a large number of small particles. In DEM, particles are approximated as rigid bodies and the interactions between them are explicitly considered [19].

4. *Body Forces:* Both gravity and buoyancy are being included in the calculation of the body force. The force is addressed by

$$\boldsymbol{F}_{grav\_i} = \boldsymbol{W}_i + \boldsymbol{F}_{boy\_i} = \frac{4}{3}\pi r_i^3 (\rho_i - \rho_f)\boldsymbol{g} \tag{11}$$
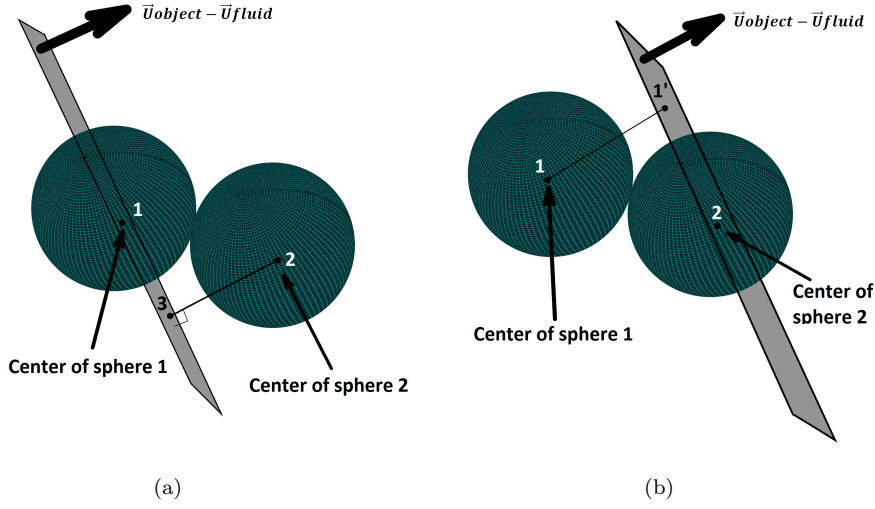
(a)   (b)

Fig. 2: a) 3 (X_3, Y_3, Z_3) stands for the projection of sphere center 2 (X_2, Y_2, Z_2)) on the plane $\mathbf{U}_{obj} - \mathbf{U}_{fluid}$ crossing sphere 1 at each center (X_1, Y_1, Z_1), and b) $1'$ $(X_{1'}, Y_{1'}, Z_{1'})$ stands for the projection of sphere center 1 (X_1, Y_1, Z_1)) on the plane $\mathbf{U}_{obj} - \mathbf{U}_{fluid}$ crossing sphere 2 at each center (X_2, Y_2, Z_2).
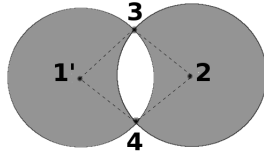

Fig. 3: Circular sector of two spheres $E_{overlapping} = domain(234) + domain(134) - E(1234)$.

where, ρ_i and ρ_f are the density of the particle i and the fluid, respectively, r_i is the radius of the particle i and $\boldsymbol{g}$ is the acceleration due to gravity.

2.2 Magnetic field and interaction domain

The magnetic field $\boldsymbol{B}$ in the MRI bore is given by

$$\boldsymbol{B} = \boldsymbol{B}_0 + \tilde{\boldsymbol{G}} + \boldsymbol{B}_1 \tag{12}$$

where, $\boldsymbol{B}_0$ is the MRI superconducting magnet field that is constant and uniform, $\tilde{\boldsymbol{G}}$ is the gradient field and $\boldsymbol{B}_1$ is the time dependent radio frequency field [20].

It is known that, the magnetic interaction force, $\boldsymbol{F}$, in the parallel direction between two spheres is inversely proportional to the fourth power of the separation
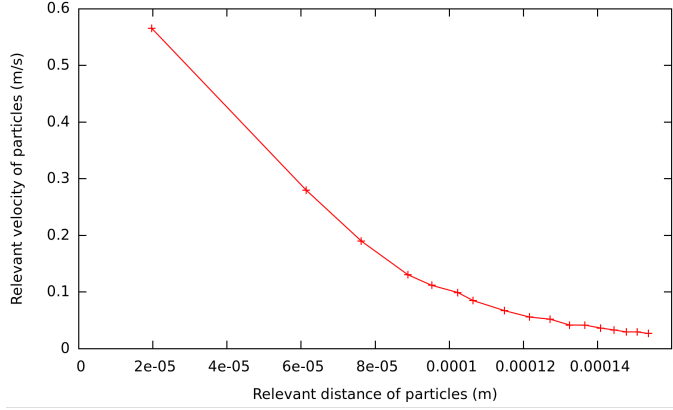
Fig. 4: Velocity of particles when approach under the force of a 1.5 T constant horizontal magnetic field from initial distance of 15 particle diameters of 11 μm.

distance [21, 22]:

$$\boldsymbol{F} \propto \frac{M_i M_j}{(h + a_i + a_j)^4} \tag{13}$$

where, M_i and M_j are the magnetic moments of the center of each sphere and h is the nearest distance between the surfaces of two spheres with radii a_i and a_j.

Although, a weak interaction is being observed for particles that are more than five radii apart, as time goes by, the interaction force is getting stronger, because the particles are getting faster close to each other, as shown in Fig. 4, for the velocity between two approaching particles. Each particle interacts with all the other which are in the same area. The magnetic interaction domain is defined by the area of the domain that the particles are located in. This is a time consuming method, because every time the magnetic moments of all particles are calculated. In order to accelerate the method, the magnetic moments that are exerted on particle i are calculated from particles that are located in distance of 15 diameters. Then, only the magnetic moments that are located in distance of 10 diameters are stored. In this way, the magnetic moments of particles that are located in distance of 10 diameters are automatically recalled in order to be used for the calculation of the magnetic moments of other particles. Simulations of 64 and 125 particles of the method which was described above show agreement in half time with the method of calculating the magnetic moments exerted on particle i from all the other particles.

2.3 Numerical Method

The OpenFoam platform was used for the calculation of the flow field and the uncoupled equations of particles motion [18]. The simulation process reads as follow: Initially, the fluid flow is found using the incompressible Navier-Stokes equations and the pressure correction method. Upon finding the flow field (pressure

Table 1: Simulation parameters

No	Concentr. (mg/ml)	Particles	Volume (m^3)	Dimensions in $(m) \times 10^4$ of $x \times y \times z$ directions			Number of cells (x,y,z)
Flow domain and computational grid of Case 1 (3D)							
1	0.563	311	4.185×10^{-10}	7.48	7.48	7.48	$34 \times 34 \times 34$
2	1.125	385	2.596×10^{-10}	6.38	6.38	6.38	$29 \times 29 \times 29$
3	2.25	336	1.133×10^{-10}	4.84	4.84	4.84	$22 \times 22 \times 22$
4	4.5	307	5.174×10^{-11}	3.96	3.96	3.30	$18 \times 18 \times 15$
Flow domain and computational grid of Case 2 (2D)							
5	25	55	2.038×10^{-13}	1.924	1.924	0.055	7×7

and velocity) the motion of particles is evaluated by the Lagrangian method by solving Eqs. (1) and (2) along the trajectory of each particle. The equations are solved in time by the Euler time marching method. The stability of the algorithm is guaranteed through a time step of the order of $10^{-6}s$.

The present numerical methods were validated against the results from Refs. [6, 13]. In order to perform the comparisons, two series of simulations with the following computational domains and grid distributions were selected: a) In the first case, four water solutions with different concentrations (0.563, 1.125, 2.25 and 4.5 in mg/ml) and by using about $300 - 400$ particles were simulated under the magnetization of a uniform magnetic field of 0.4 T in a stationary fluid. The spacing of the $3D$ computational grid of this case was 2 × diameter of the particle in each direction. b) In the second case, a solution with concentration of 25 mg/ml of 55 polystyrene magnetic particles with diameter of 5.5 μm was simulated in distilled stationary water under a constant magnetic field of $0.005T$ and a gradient magnetic field of $\tilde{G} = 1.4$ T/m along the $x-$axis. The spacing of the $2D$ domain was 5 × diameter of the particle in each direction. The summary of the domain parameters for the first and the second case is shown in Table 1.

3 RESULTS

Two series of simulations were performed according to the parameters that are described in the previous section. In the first case, which is initially addressed by Mathieu and Martel [6], the aggregation of Fe_3O_4 particles dispersed in a stationary distilled water is investigated under the influence of a constant magnetic field. The density of the particle and the fluidic environment was 1087 kg/m^3 and 1000 kg/m^3, respectively, while the diameter of the particles was considered to be 11 μm. The relative magnetic permeability of the Fe_3O_4 particles was 12.3 and the magnetic permeability of the fluid was $4\pi \times 10^{-7}$ A/m. The Young's modulus of the material was 10^9 N/m^2, the tangential stiffness was 10 Nsm^{-1} and the coefficient of friction and the Poisson ratio was 0.5 for the two properties.

Four water solutions with particle concentrations of 0.563 mg/ml, 1.125 mg/ml, 2.25 mg/ml and 4.5 mg/ml were simulated under a uniform transverse magnetic field of magnitude $B_0 = 0.4$ T. No external magnetic gradient is applied during this simulation and the initial positions of the microparticles are randomly generated. At the beginning of each simulation, for $t = 0s$, the magnetic field is $B_0 = 0$ T and under the influence of the uniform magnetic field the particles (magnetic
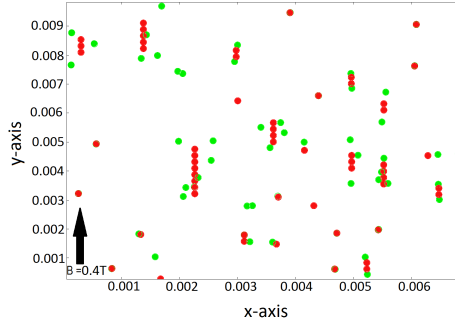
Fig. 5: Green (lighter) particles are shown the initial particle position at $t = 0s$, while red (darker) particles correspond to $t = 5\ ms$ where the particles chains are fully formed parallel to the steady magnetic field.

dipoles) are formed into chains that are oriented parallel to the magnetic field within $t = 5\ ms$, as it is shown in Fig. 5.

Due to the external magnetic field, the magnetic particles are acting like magnets and the particle motion is attributed to gravity and magnetic interactions forces, since no fluid flow exists. The size of the aggregations that are formed as a function of particle numbers and concentrations is presented in Table 2. Results from concentration 1.125 mg/ml, for example, show that four aggregates of length 10 particles may be formed due to the application of this magnetic field. It is observed that the size of the aggregations is increased as concentration increases and for 4.5 mg/ml aggregates of 35 particles may be found. The results from the simulation are compared against the experimental data of Ref. [6] as it is depicted in Fig. 6 and tabulated in Table 3 for the mean length of the aggregates and their standard size deviation.

Figure 6 shows the length of aggregates major axis whose average value follows an upward trend as a function of suspension concentration. The major axis length corresponds to the longest dimension of the aggregates measured. Larger aggregates are detected in increasing numbers as the concentration of the suspension increases. For the concentration of 0.563 mg/ml the numerical results are very close to the experimental, while for the concentration of 1.125 mg/ml results are similar compared to the experimental data in terms of mean length. For the higher concentrations an underestimation may be observed between the results of simulations and the experimental one. This difference is due to the small numbers of particles (up to 380 particles) that were used in the simulation in comparison in contrast to the measurements that were conducted using a number of particles in the order of 10^6.

The second case that is studied here, which is initially addressed by Vartholomeos and Mavroidis [13], investigates the flow and aggregation of particles under the combine action of a constant and a gradient external magnetic field acting si-
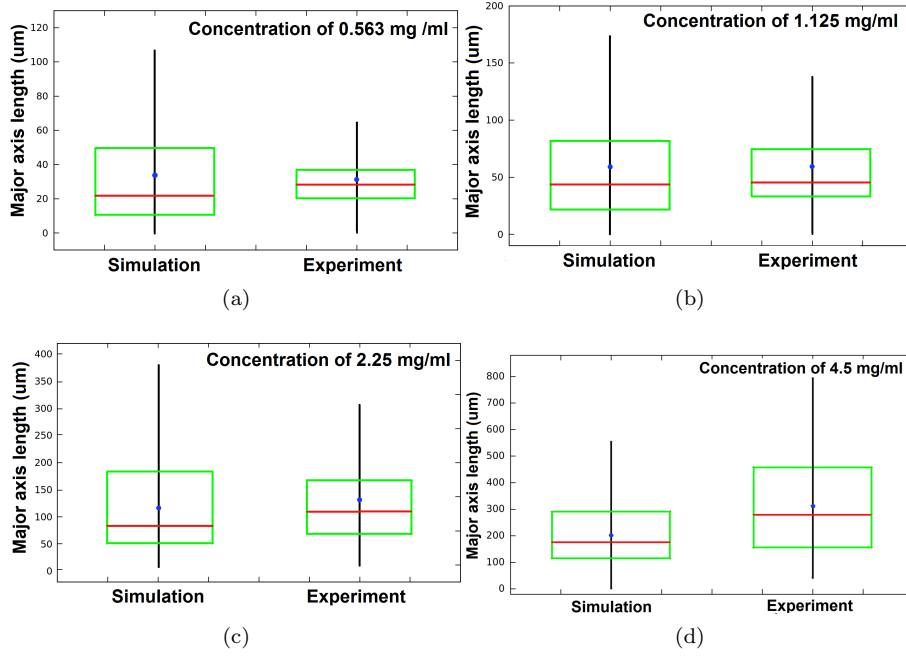
Fig. 6: Box plots show variations in the major axis length of aggregates from the present simulations and the measurements of Ref. [6]. The boxes captures the lower quartile, median (red line) and upper quartile values. The black line that extended from the box show the upper and the lower fence. The blue dots shows the average length of the aggregations in each case. a) 0.563 mg/ml, b) 1.125 mg/ml, c) 2.25 mg/ml, and d) 4.5 mg/ml.

multaneously. The present results were compared against the experimental measurements and simulations of [13] for the motion of a magnetic suspension of polystyrene magnetic particles (5.5 μm) with density of 1050 kg/m^3 and concentration of 25 kg/m^3 in distilled water.

Driven by the uniform magnetic field and the magnetic gradient along the $x-$axis, the microparticles are successively aggregated and simultaneously transported in the direction of the magnetic gradient. Four instances of the particle locations that show their motion and the mechanism of the formation of the aggregates are presented in Fig. 7. Depending of their close neighbors positions, particles may approach others or stay isolated. The duration for the formation of the aggregates is $t = 1.25s$ as depicted in Fig. 7, and for larger times only translational motion of the aggregates is found. Thus, as it is expected, it is found that longer time is needed for the formation of aggregates than in the first case studied due to the slower magnetic forces from the weaker horizontal constant magnetic field. The results of the present simulation are summarized and compared against the experimental data and simulations of Ref. [13] in Table 4.

It is observed that the present results show good qualitative and quantitative agreement mainly in terms of the mean velocity and the mean length of aggrega-

Table 2: Summary of the results from Case 1

	Particles per simulation			
	311	385	336	307
Particles per aggregation	0.563 *mg/ml*	1.125 *mg/ml*	2.25 *mg/ml*	4.5 *mg/ml*
1	26	9	0	0
2	24	13	3	0
3	18	5	3	1
4	5	11	3	1
5	7	5	3	0
6	7	6	2	0
7	7	5	3	0
8	2	4	0	0
9	2	2	2	1
10	1	4	2	1
11	0	2	11	1
12	0	2	0	2
13	0	1	0	0
14	0	0	1	0
15	0	0	0	1
16	0	0	2	0
17	0	1	0	1
18	0	0	2	0
19	0	1	0	0
21	0	0	1	0
23	0	0	1	1
25	0	0	1	0
26	0	0	0	2
27	0	0	0	1
31	0	0	0	1
32	0	0	1	1
35	0	0	0	1

Table 3: Comparison of the present results against the experimental measurements from Ref. [6].

Concentr. (mg/ml)	Particle number	Mean length (μm)	std	Mean length (μm)	std
-	-	simulation	sim.	experiment	exp.
0.563	311	34.02	23.72	31	16
1.125	385	59.14	43.19	59	36
2.25	336	108.93	83.79	137	85
4.5	307	201.49	109.42	317	195

tions in comparison to the experimental one. The small number of particles that is used in the experiment and the simulation is probably the source of the small difference in the comparison because initial locations of particles may be crucial for the formation and motion of chains. Moreover, results may be influenced also by the diameter of the particles that was kept constant in the present simulation, while in the experiment had a normal distribution. Consequently, existing small particles were easier and faster concentrated around bigger particles and thus bigger chains of aggregations may be formulated.

Table 4: Comparison of experimental and simulation results for Case 2

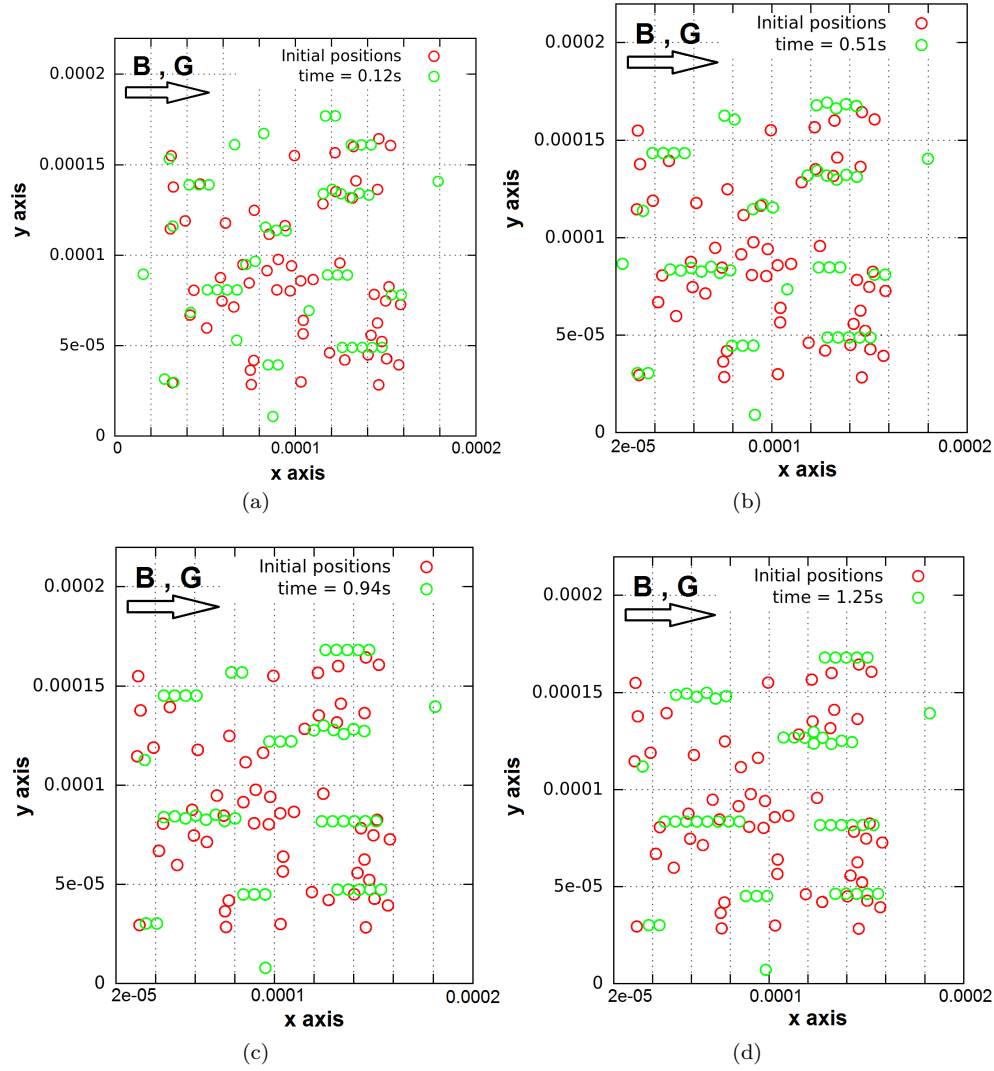| Case	Mean size (particles)	std size (particles)	Mean velocity ($\mu m/s$)	std velocity ($\mu m/s$)
Experiment, Ref. [13]	7	5	7.5	1
Present	5.26	1.89	8.3	1.4
Numerical, Ref. [13]	10	4	9	2

Fig. 7: Staring positions of particles (red circles) and final positions (green circles) for particles displacement between $t = 0\ s$ and: a) $t = 0.12\ s$, b) $t = 0.51\ s$, c) $t = 0.94\ s$, and d) $t = 1.25\ s$.

4 DISCUSSION

In this study, we were able to validate a new numerical model for the MRI guided drug delivery system that is based on magnetic nanoparticle aggregations for the navigation of paramagnetic nanocupsules. The present method is based on computational fluid dynamics and it is as general as possible and thus can be easily extended for use under realistic in-vitro or in-vivo conditions. The purpose of this work is to examine under which conditions the model is reliably working. For this reason, two basic particle suspension flows were selected where particles are influenced by a constant and in the second case a gradient magnetic field.

Simulations with the present method is more expensive as the number of particles increases because magnetic moments should be calculated for every particle and for every time step. However, given a particle suspension and the magnitude of the external magnetic field the method can be applied and provide very good accuracy for the prediction of the size of conglomerates. As it is observed from Table 3, when the ratio of the number of the particles to the suspension concentration is high, numerical results are very close to the experimental. As this ratio decreases, the method underestimates the size of the aggregations but still is capable to predict qualitatively their growth.

An important advantage of this work is also that the developed model is found to predict more accurate the dynamics of the aggregates than other simulations with similar models as Table 4 presents. Results show that the most important quantity for the driving of the nanoparticles, i.e. the mean velocity which is developed under gradient magnetic fields, is very closely predicted to the experimental values. This improved feature of the proposed model is due to the evaluation of the more realistic aerodynamic coefficient $C_d A_{eff}$ that incorporates the effect in the drug from the exposed shape of the aggregates in a better way, since it is general true that $C_d A_{eff} < C_d A$.

5 CONCLUSION

A numerical model for the simulation of magnetically guided drug delivery was developed in order to predict the motion of magnetic particles for medical applications. This method aims at predicting the aggregation's procedure and the velocity of each particle inside the arteries and arterioles of a human body. It aims also at simulating the motion of aggregations when these are driven by MRI magnetic gradient coils. A novel method is developed for the calculation of the drag coefficient that takes into account the exposed area of the particle in the fluid.

The method was tested through comparison against experimental and numerical data. It was found that the present method can simulate satisfactory the experiments in a stationary fluid under a steady magnetic field. Furthermore, the model was tested for the acceleration of aggregated particles under the influence of a constant and a superimposed gradient magnetic field. The results were very close to existing experimental data in terms of velocity and aggregation size and comparable to the results from existing simulations.

Acknowledgments

References

1. A. Senyei, K. Widder, and C. Czerlinski, "Magnetic guidance of drug carrying microspheres," *Appl. phys.*, vol. 49, pp. 3578–83 (1978).
2. K. Widder, A. Senyei, and G. Scarpelli, "Magnetic microspheres : a model system of site specific drug delivery in vivo." *Proc. Soc. Exp. Biol. Med.*, vol. 158, pp. 141–6 (1978).
3. J. Llandro, J. J. Palfreyman, A. Ionescu, and C. H. W. Barnes, "Magnetic biosensor technologies for medical applications: a review," *Med. Biol. Eng. Comput.*, vol. 48, pp. 977–998 (2010).
4. K. Widder, P. Marino, R. Morris, and A. Senyei, *In: Targeted Drugs, Goldberg E (Ed.).* NY, USA: John Wiley and Sons (1983).
5. Q. Pankhurst, J. Connolly, S. Jones, and J. Dobson, "Applications of magnetic nanoparticles in biomedicine," *Physiscs D:Applied Physics*, vol. 36, pp. 166–181 (2003).
6. J.-B. Mathieu and S. Martel, "Aggregation of magnetic microparticles in the context of targeted therapies actuated by a magnetic resonance imaging system," *J. Appl. Phys.*, vol. 106, p. 044904 (2009).
7. P. Babinec, A. Krafcik, M. Babincova, and J. Rosenecker, "Dynamics of magnetic particles in cylindrical halbach array: implications for magnetic cell separation and drug targeting," *Med. Biol. Eng. Comput.*, vol. 48, pp. 745–753 (2010).
8. K. van Netten, K. Galvin, and J. hou, "Magnetically driven hydrodynamic interactions of magnetic and non-magnetic particles," *Chemical Engineering science*, vol. 63, pp. 3431–3437 (2008).
9. K. V. Netten, J. hou, K. Galvin, and R. Moreno-Atanasio, "Influence of magnetic and hydrodynamic forces on chain-aggregation and motion of magnetisable particles and composites," *Chemical Engineering science*, vol. 93, pp. 229–237 (2013).
10. B. Gleich, N. Hellwig, H. Bridell, R. Jurgons, C. Seliger, C. Alexiou, B. Wolf, and T. Weyh, "Design and Evaluation of Magnetic Fields for Nanoparticle Drug Targeting in Cancer," *IEEE Transactions on nanotechnology*, vol. 6, pp. 164–170 (2007).
11. T. Kubo, T. Sugita, and S. Shimose, "Targeted delivery of anticancer drugs with intravenously administreted magnetic lipomes in osteosarcoma- bearing hamsters," *Int. J. Oncol.*, vol. 17, pp. 309–16 (2000).
12. B. Yellen, Z. Forbes, and D. Halverson, "Targeted drug delivery to magnetic implants for therapeutic applications," *Magn. Magn. Mater*, vol. 293, pp. 647–54 (2005).
13. P. Vartholomeos and C. Mavroidis, "In silico studies of magnetic microparticle aggregations in fluid environments for MRI-guided drug delivery," *IEEE transactions on biomedical engineering*, vol. 59, no. 11, pp. 3028–3038 (2012).
14. K. W. Yung, P. B. Landecker, and D. D.Villani, "An analytic solution for forces between two magnetic dipoles," *Magn. Elect. Sep.*, vol. 20, pp. 39–52 (1998).
15. E. Climent, M. Maxey, and G. E.Karniadakis, "Dynamics of self-assembled chaining in magnetorheological fluids," *Langmuir*, vol. 20, pp. 507–513 (2004).
16. J. D. Jackson, *Classical Electrodynamics, 3rd ed.* Hoboken,NJ: Wiley (1999).
17. M. Karimi, G. Akdogan, K. H. Dellimore, and S. M. Bradshaw, "Comparison of different drag coefficient correlations in the CFD modelling of a laboratory-scale ruschton-turbine flotation tank," pp. 1–7 (2012).
18. OpenFoam Manual. Available Online: `http://www.openfoam.org`
19. E. Tijskens, H.Ramon, and J. Baerdemaeker, "Discrete element modelling for process simulation in agriculture," *J. of Sound and Vibration*, vol. 266, pp. 493–514 (2003).
20. C. L. Epstein and F. W. Wehrli. (2005) Magnetic resonance imaging. [Online]. Available: `http://www.math.upenn.edu`

21. A. Mehdizadeh, R. Mei, J. F. Klausner, and N. Rahmatian, "Interaction forces between soft magnetic particles in uniform and non-uniform magnetic fields," *Acta Mechanica Sin.*, vol. 26, pp. 921–929 (2010).
22. T. Fujita and M. Mamiya, "Interaction forces between nonmagnetic particles in the magnetized magnetic fluid," *J. of Magnetism and Magnetic Materials*, vol. 65, pp. 207–210 (1987).